

Photoluminescence from Single-Walled MoS₂ Nanotubes Coaxially Grown on Boron Nitride Nanotubes

Ming Liu¹, Kaoru Hisama¹, Yongjia Zheng¹, Mina Maruyama², Seungju Seo¹, Anton Anisimov³,
Taiki Inoue^{1,4}, Esko I. Kauppinen⁵, Susumu Okada², Shohei Chiashi¹, Rong Xiang¹, and Shigeo
Maruyama^{1*}

¹ *Department of Mechanical Engineering, The University of Tokyo, Tokyo 113-8656, Japan*

² *Graduate School of Pure and Applied Sciences, University of Tsukuba, Tsukuba 305-8571,
Japan*

³ *Canatu Ltd., Helsinki FI - 00390, Finland*

⁴ *Department of Applied Physics, Graduate School of Engineering, Osaka University, Osaka
565-0871, Japan*

⁵ *Department of Applied Physics, Aalto University School of Science, Espoo 15100, FI-00076
Aalto, Finland*

*email: maruyama@photon.t.u-tokyo.ac.jp

Abstract

Single- and multi-walled molybdenum disulfide (MoS_2) nanotubes have been coaxially grown on small diameter boron nitride nanotubes (BNNTs) which were synthesized from heteronanotubes by removing single-walled carbon nanotubes (SWCNTs), and systematically investigated by optical spectroscopy. The strong photoluminescence (PL) from single-walled MoS_2 nanotubes supported by core BNNTs is observed in this work, which evidences a direct band gap structure for single-walled MoS_2 nanotubes with around 6 - 7 nm in diameter. The observation is consistent with our DFT results that the single-walled MoS_2 nanotube changes from an indirect-gap to a direct-gap semiconductor when the diameter of a nanotube is more than around 5 nm. On the other hand, when there are SWCNTs inside the heteronanotubes of BNNTs and MoS_2 nanotubes, the PL signal is considerably quenched. The charge transfer and energy transfer between SWCNTs and single-walled MoS_2 nanotubes were examined through characterizations by PL, XPS, and Raman spectroscopy. Unlike the single-walled MoS_2 nanotubes, multi-walled MoS_2 nanotubes do not emit light. Single- and multi-walled MoS_2 nanotubes exhibit different Raman features in both resonant and non-resonant Raman spectra. The method of assembling heteronanotubes using BNNTs as templates provides an efficient approach for exploring the electronic and optical properties of other transition metal dichalcogenide nanotubes.

Introduction

Van der Waals heterostructure of two-dimensional (2D) layered materials¹ have attracted much attention in material research since the first experimental isolation of single-layer graphene.²⁻⁷ The novel properties in heterostructures with diverse layerings of metal, semiconductors or insulators have raised numerous new designs of electronic devices as well as optoelectronic devices. Atomically thin transition-metal dichalcogenide (TMD) such as MoS₂ holds great promise for electrical, optical, and mechanical devices, as well as novel physical phenomena.⁸ Meanwhile, wrapping 2D TMD materials into 1D nanotubes has brought interests in creating chiral tubular structure and radial heterojunctions with diverse functionalities.⁹ Recently, we have demonstrated one-dimensional (1D) van der Waals heterostructures templated on single-walled carbon nanotubes (SWCNTs).¹⁰ 1D van der Waals materials will join the innovation of electronic and optoelectronic devices with 2D layered materials.

Fullerene-like and nanotube structures of MoS₂ have been produced by a gas-phase reaction firstly in 1995.¹¹ A combined theoretical and experimental work has indicated that multi-walled MoS₂ nanotubes are more stable than single-walled MoS₂ nanotubes, while single-walled MoS₂ with diameter more than about 6 nm is more stable than nanoribbon shape.¹² The conventional growth process has resulted in multi-walled MoS₂ nanotubes with large diameters.^{11, 13} The bulk form of MoS₂ is an indirect band gap semiconductor with an energy gap of ~1.2 eV¹⁴ and has attracted attention as photovoltaic and photocatalytic materials.^{15, 16} The band gap of MoS₂ changes from indirect to direct when the thickness reduces to a single layer.¹⁷ In addition, recent studies have showed the strong photoluminescence in monolayer MoS₂ that can be attributed to the direct gap electronic structure.¹⁸⁻²⁰ The band structure of single-walled and multi-walled MoS₂ nanotubes are still not well investigated experimentally, though modulated calculations have predicted that MoS₂ nanotubes have indirect band gaps except those with zigzag chiral indices.²¹⁻²³ Here, although the zigzag MoS₂ nanotubes are calculated as direct-gap semiconductors, the band edge states are predicted to come from different subbands and PL is not expected.²⁴

Using a tubular template to confine the formation of inorganic nanotubes has been proposed to stabilize few-walled inorganic nanotubes, which is a critical step toward understanding their optical properties and implementing into novel devices. Carbon nanotubes (CNTs) have been used as a template to assemble specific materials^{25, 26} and as filling vessels for metals^{27, 28} for forming

core-shell nanotubes. Charge transfer from a CNT core to a MoS₂ sheath has been verified by X-ray photoelectron spectroscopy in a composite MoS₂/CNT material.²⁹ The ultrafast optoelectronic processes in 1D heterostructures have been investigated lately.³⁰ Core-shell carbon@MoS₂ nanotube sponges have been utilized as electrodes in a high-performance battery.³¹ However, single-walled MoS₂ nanotubes are not observed in the previous core-shell inorganic nanotube studies. Besides, CNTs are optically active materials with high response signal of Raman spectra³² and photoluminescence spectra,³³ which makes the investigation of optical properties of the TMD shell outside a CNT infeasible. Hence, boron nitride nanotube (BNNT) is a promising substitute for serving as a template for forming MoS₂ nanotubes since the band gap of BNNTs is ~5.5 eV which is large enough to be transparent within a wide range of wavelengths and quasi-independent from the chirality.³⁴

In this paper, we present a systematic study of the optical properties and electronic structure of MoS₂ nanotubes including single-walled and multi-walled types. We have developed a facile chemical vapor deposition (CVD) method for synthesizing core-shell boron nitride and MoS₂ heteronanotubes (BNNT@MoS₂NT) by removing the SWCNTs in heteronanotubes of SWCNTs coated by BNNT (SWCNT@BNNT). The hetero structure based on BNNTs is a promising platform for studying the optical properties of MoS₂ layers or other TMD layers. The properties of BNNT@MoS₂NT heteronanotubes were examined by using three complementary spectroscopic techniques: optical absorption, Raman spectroscopy, and photoluminescence (PL), with additional characterizations provided by transmission electron microscopy (TEM) and DFT calculations using the STATE (Simulation Tool for Atom Technology) package. The strong PL signal from single-walled MoS₂ nanotubes indicates the direct band gap structure of the material, which is consistent with our DFT results. With increasing the wall number of MoS₂ nanotubes, the PL signal decreased significantly which allows us to trace the direct and indirect band gaps structures of the MoS₂ nanotubes. The charge and energy transfer between SWCNTs and MoS₂ nanotubes in the 1D hetero structure were observed in this work.

Results and Discussion

Synthesis and structure analysis of BNNT@MoS₂NT heteronanotubes. In this work, we presented a template-assisted approach involving a sequence of facile CVD processes using SWCNTs as a template to produce BNNT@MoS₂NT heteronanotubes. The SWCNT film prepared by areosol CVD was used as a template and transferred onto a ceramic washer with the size of 4 mm inner diameter and 6 mm outer diameter. Firstly, the suspended SWCNT film on the washer was used as a template and ammonia borane was employed as the precursor to form a coaxial tube structure of SWCNT coated by boron nitride nanotubes (SWCNT@BNNT). Then the SWCNT@BNNT film was annealed at 610°C in the oxygen atmosphere with the pressure of 85 kPa for 12 hours to remove the SWCNTs in the film. The optical image of the as-synthesized BNNT film after the annealing process is shown in Figure 1a. The BNNT film is fully transparent within the visible range of wavelengths, which is confirmed by the absorption spectrum in Figure S1a. The Raman peak at $\sim 1370\text{ cm}^{-1}$ was detected in Figure S1b, which is corresponding to the E_{2g} in-plane vibrational mode of the h-BN networks. The Raman peak at 1555.5 cm^{-1} in Figure S1b is the vibrational mode of oxygen. In the Fourier transformed infrared (FT-IR) spectrum (Figure S1c), the absorption band at $\sim 1369.5\text{ cm}^{-1}$ is attributed to the in-plane stretching mode of

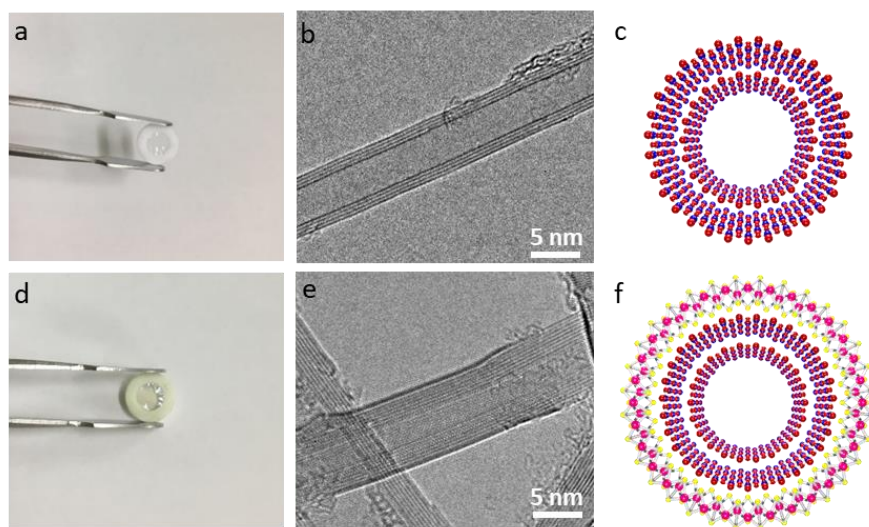


Figure 1. (a) Optical image of the suspended BNNT film on a ceramic washer. (b) Representative high-resolution TEM image of a multi-walled BNNT. (c) Atomic model of a multi-walled BNNT. (d) Optical image of the suspended BNNT@MoS₂NT nanotubes film on a ceramic washer. (e) Representative high-resolution TEM image of a BNNT@MoS₂NT. (f) Atomic model of a BNNT@MoS₂NT.

the h-BN that vibrates along the longitudinal or tube axis of a BNNT. Besides, the peak at ~ 1520 cm^{-1} corresponds to the stretching of the h-BN along the tangential directions of a BNNT. This stretching mode smears out for h-BN bulks or thin films, and only shows up when the tube curvature induces an anisotropic strain on the h-BN which indicates the high crystallinity of BNNTs.³⁵ The representative high-resolution TEM image and the atomic model of a high quality BNNT are presented in Figure 1, b and c. The as-synthesized BNNT film on a ceramic was a template for the MoS₂ CVD process to form the BNNT@MoS₂NT heteronanotubes. The MoS₂ CVD was conducted at 530 °C with the sulfide and MoO₃ powders as precursors. The typical growing time of MoS₂ at 530 °C is 10 min and the optical image of BNNT@MoS₂NT film is shown in Figure 1d. In Figure 1e, the representative TEM image of the BNNT@MoS₂NT, the diameter of the outer layer MoS₂ nanotube is around 6.8 nm and the inner diameter of the multi-walled BNNT is 2.1 nm. The atomic model of a BNNT@MoS₂NT heteronanotube is presented in Figure 1f. In the BNNT@MoS₂NT heteronanotube, there is no chemical bonding between BN layer and MoS₂ layer.

Photoluminescence from single-walled MoS₂ nanotubes and the charge and energy transfer between SWCNT and MoS₂ nanotubes. Figure 2a shows the atomic model of two types of heteronanotubes that we used to compare, SWCNT@BNNT@MoS₂NT and BNNT@MoS₂NT heteronanotubes. The PL, Raman, and absorption spectra of the two heteronanotubes are compared in Figure 3b, 3c, and 3d, respectively. The SWCNT@BNNT@MoS₂NT heteronanotube was synthesized by the serial CVD method described in our previous work.¹⁰ The representative TEM image of the SWCNT@BNNT@MoS₂NT heteronanotube is shown in Figure S2. Optical measurements by PL, Raman, and absorption spectroscopy were performed on the free-standing SWCNT@BNNT@MoS₂NT and BNNT@MoS₂NT heteronanotube films on ceramic washers. All optical measurements were conducted under ambient conditions at room temperature. The excitation wavelength of Raman and PL spectroscopy was 532 nm (2.33 eV) with a spot diameter of ~ 2 μm focused on the sample. A low laser power of ~ 70 μW (out of the microscope) was applied to avoid heating and PL saturation.³⁶ Appreciable PL was observed from single-walled MoS₂ nanotubes coaxially grown on BNNTs, the BNNT@MoS₂NT samples. The measured PL intensities for a BNNT@MoS₂NT and a SWCNT@BNNT@MoS₂NT sample under the identical excitation at 2.33 eV are significantly different (Figure 2b). The PL intensity of

SWCNT@BNNT@MoS₂NT sample is eight times less than the PL signal from the BNNT@MoS₂NT sample. However, the shape of the normalized PL spectra for both samples are nearly identical. The PL spectrum of BNNT@MoS₂NT consists a single feature centered at 1.85 eV. In contrast, the center of the PL peak for SWCNT@BNNT@MoS₂NT is at 1.87 eV, slightly blue shifted. The sharp peaks in both PL spectra are from the Raman signal of the MoS₂ and SWCNT in the film.

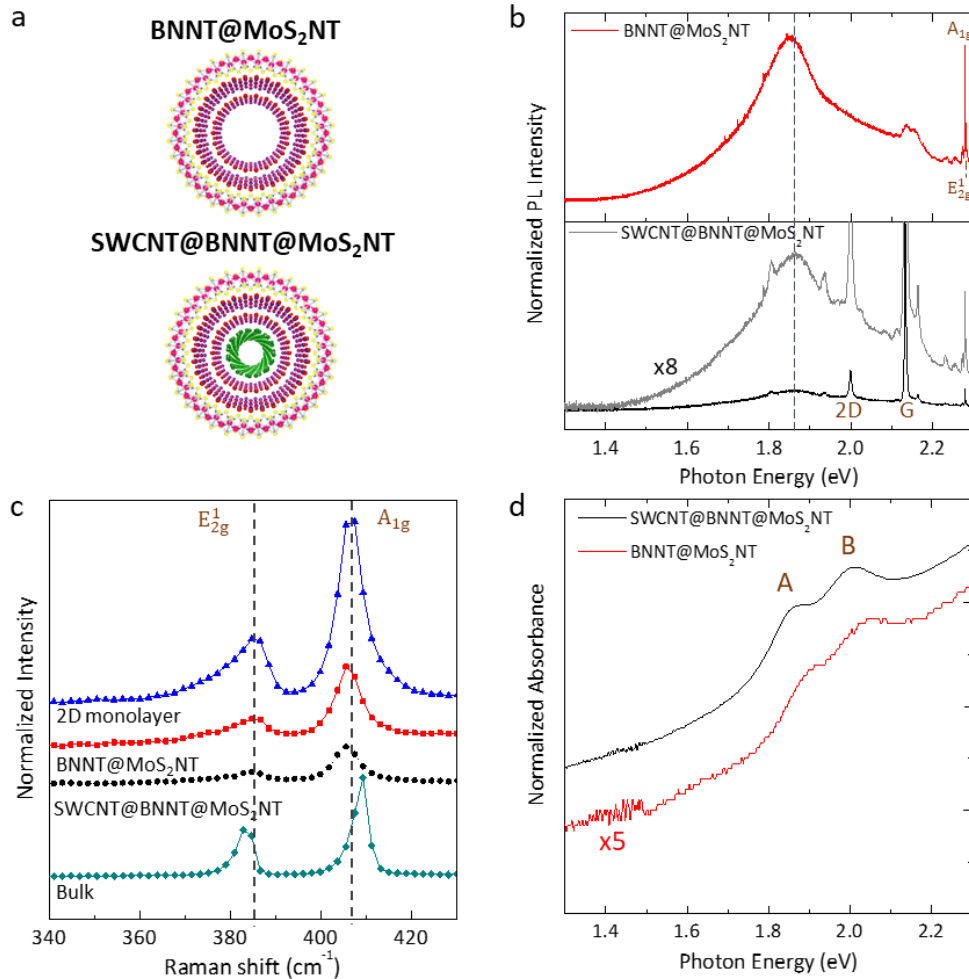


Figure 2. (a) The atomic model of a SWCNT@BNNT@MoS₂NT heteronanotube and a BNNT@MoS₂NT heteronanotube. (b) The PL spectra of BNNT@MoS₂NT and BNNT@MoS₂NT, respectively. The black dot line is the eight times enlarged PL spectrum of SWCNT@BNNT@MoS₂NT. (c) Representative Raman spectra of 2D monolayer MoS₂, BNNT@MoS₂NT, SWCNT@BNNT@MoS₂NT, and bulk MoS₂. (d) Representative absorption spectra of free-standing SWCNT@BNNT@MoS₂NT and BNNT@MoS₂NT films.

To understand the origin of the extraordinary PL property from single-walled MoS₂ nanotubes, we compared the PL spectra with the absorption spectra of these samples (Figure 2d). In the range of 1.3–2.3 eV, there are two main absorption peaks that are contributed to the direct-gap transitions between the maxima of split valence bands (ν_1 and ν_2) and the minimum of the conduction band (c_1) which are all located at the K point of the Brillouin zone.³⁷⁻³⁹ The PL peak of BNNT@MoS₂NT at 1.85 eV matches the lower absorption resonance (conventionally called A exciton) in the absorption spectrum. Therefore, we assigned the PL of BNNT@MoS₂NT to direct-gap luminescence. The upper absorption resonance (B exciton) is observed in SWCNT@BNNT@MoS₂NT and BNNT@MoS₂NT, however the PL emission from B exciton is not observed in our experiment.

The PL quenching in the SWCNT@BNNT@MoS₂NT sample is significant compared with the PL of BNNT@MoS₂NT. The near-field coupling, for example interlayer charge and/or energy transfer, is the main reason for causing the PL quenching effect.⁴⁰ To analyze the interaction between the SWCNT and MoS₂, we converted the PL spectrum of SWCNT@BNNT@MoS₂NT to the Raman scale and enlarged PL peak for both samples (Figure S3). In Figure S3a, there is a noticeable blue shift of the PL from SWCNT@BNNT@MoS₂NT compared with the PL from BNNT@MoS₂NT which verifies the photoinduced hole doping (p-dope) in MoS₂ nanotubes.^{41, 42} The Raman spectrum of SWCNT in SWCNT@BNNT@MoS₂NT heteronanotubes (Figure S3b black line) presents the typical electron doping (n-dope) effect based on the downshift of the G and 2D peak position.^{43, 44} In the XPS spectra (Figure S3c), the C1s peak of SWCNT@BNNT@MoS₂NT heteronanotubes presents 0.2 eV shifting to higher binding energy compared with the C1s peak of pristine SWCNT film which also proves the n-dope of SWCNT in the heteronanotubes. Therefore, in SWCNT@BNNT@MoS₂NT heteronanotubes, the net electron transfers from MoS₂ nanotubes to SWCNT causing the n-dope of SWCNT, and which naturally implies hole accumulated in MoS₂ resulting in the doping to the p-direction of MoS₂ nanotubes. Hence, charge transfer occurs between SWCNT and MoS₂ nanotubes in SWCNT@BNNT@MoS₂NT heteronanotubes. Although electrons may transfer to SWCNT referring to the demonstration from our experimental data, the interlayer charge transfer processes alone cannot be responsible for the massive PL quenching. Instead, interlayer energy transfer provides a highly efficient relaxation pathway⁴⁰ for excitons in SWCNT@BNNT@MoS₂NT heteronanotubes. Therefore, in SWCNT@BNNT@MoS₂NT heteronanotubes, charge transfer and

energy transfer may happen at the same time. More detailed investigations need to be applied to confirm the hypothesis.

Raman spectra of 2D monolayer MoS₂, BNNT@MoS₂NT, SWCNT@BNNT@MoS₂NT, and bulk MoS₂ are shown in Figure 2c. The in-plane E_{2g}¹ and out-of-plane A_{1g} Raman modes of MoS₂ were observed in our BNNT@MoS₂NT and SWCNT@BNNT@MoS₂NT samples. The frequencies of both modes in single-walled MoS₂ nanotubes in heteronanotubes are almost same as the monolayer MoS₂ values. The frequency difference of two modes is about 21 cm⁻¹ which is identical with the monolayer MoS₂ sample. From the previous study, the E_{2g}¹ vibration softens (red shifts), while the A_{1g} vibration stiffens (blue shifts) with increasing thickness of 2D MoS₂ films.⁴⁵ However, we did not observe any clear softening or stiffening of the Raman modes in single-walled MoS₂ nanotubes compared with monolayer MoS₂ though the curvature and strain energy in nanotubes are different.

Band structure of single-walled MoS₂ nanotubes. A monolayer MoS₂ is well known as a semiconductor with a direct band gap at the K point in the Brillouin zone,¹⁹ while MoS₂ nanotubes have been predicted as a semiconductor with an indirect band gap except zigzag types.²¹ In the previous studies, the band edge is based on the effect of strain from the curvature, which induces an increase of the energy levels of valence bands around Γ point that forms an indirect band gap with the bottom of the conduction band originated from the monolayer K point. For the zigzag MoS₂ nanotubes, however, they have direct band gaps because the K and Γ points are folded at the same place in the one-dimensional Brillouin zone of a nanotube. Because this special folding is only possible for the zigzag nanotube, all chiral nanotubes are expected behave as armchair nanotubes.²² Here we suspected that the effect of the strain would decrease as the diameter of a nanotube becomes larger. When the diameter of a nanotube reached a certain size, reduced strain would make the band gap of a nanotube approach the direct band gap as a monolayer MoS₂. Figure 3 presents the electronic structure of three types of single-walled MoS₂ nanotubes with chiral indices of (12,12), (24,24), and (36,36) that are calculated by a density functional theory.^{46,47} The energy is measured with respect to that of the valence band edge at the Γ point. The valence peak at near $k = 2\pi/3$, originated from the K point of the Brillouin zone, becomes higher when the diameter of the nanotube increases. For the chiral index of (36,36) with diameter about 6.3 nm, the band structure of a nanotube forms a direct bang gap as in Fig. 3c. The detailed discussion of the

band gap crossover for MoS₂ nanotubes will be reported in another paper.⁴⁸ The result in our paper⁴⁸ shows when the diameter of a MoS₂ nanotube is larger than 5 nm, the nanotube is a semiconductor with a direct band gap which corresponds with the strong PL signal observed in the BNNT@MoS₂NT heteronanotube in this paper.

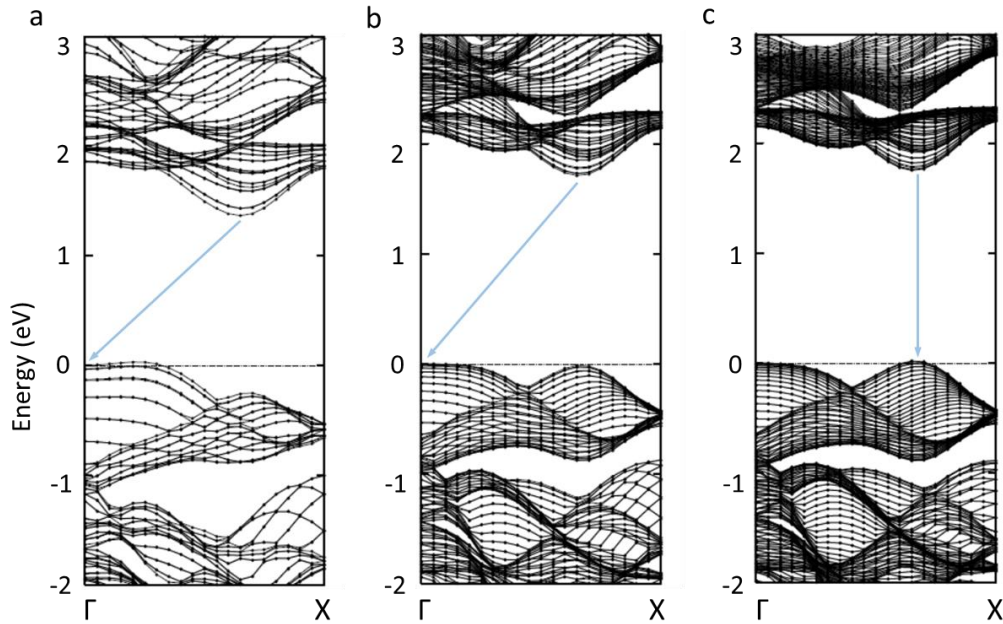


Figure 3. Calculated electronic structure of MoS₂ nanotubes with different indices (a) (12,12) with diameter of 2.1 nm, (b) (24,24) with diameter of 4.2 nm, and (c) (36,36) with diameter of 6.3 nm.

Structure of BNNT@single-MoS₂NT and BNNT@multi-MoS₂NT heteronanotubes.

The heteronanotubes of single-walled MoS₂ nanotubes coaxially grown on BNNTs (BNNT@single-MoS₂NT) were systematically characterized by optical measurements for example PL, Raman spectroscopy, and absorption. Here, multi-walled MoS₂ nanotubes coaxially grown on BNNTs (BNNT@multi-MoS₂NT) were synthesized by modifying the MoS₂ CVD parameters for studying the difference of the optical properties between BNNT@single-MoS₂NT and BNNT@multi-MoS₂NT nanotubes. The representative TEM images of BNNT@single-MoS₂NT and BNNT@multi-MoS₂NT nanotubes are shown in Figure S4. In Figure S4a, the MoS₂ nanotubes coaxially grown on BNNTs are single-walled nanotubes, whereas the MoS₂ nanotubes in Figure S4b have two or three walls. These two types of samples were used in the following optical characterizations.

The comparison of Raman, PL, and absorption spectra of BNNT@single-MoS₂NT and BNNT@multi-MoS₂NT heteronanotubes. Figure 4a shows representative Raman spectra of BNNT@single-MoS₂NT and BNNT@multi-MoS₂NT samples with the excitation wavelength of 532 nm in air ambient environment. The E_{2g}^1 and A_{1g} modes were observed in both BNNT@single- and BNNT@multi- MoS₂NT samples. The in-plane E_{2g}^1 mode is associated with opposite vibration of two S atoms with respect to the Mo atom, whereas the out-of-plane A_{1g} mode originates from the vibration of S atoms in opposite directions.^{49, 50} For BNNT@single-MoS₂NT sample, the peak of the A_{1g} mode is at 405 cm⁻¹ and the E_{2g}^1 mode locates at 384 cm⁻¹. Strikingly, we found the E_{2g}^1 vibration softened to ~380 cm⁻¹ (red shifts), while the A_{1g} mode remained at the same position (~405 cm⁻¹) in the BNNT@multi-MoS₂NT sample. When the wall number increases, the interlayer van der Waals force in MoS₂ suppresses atom vibration, resulting in higher force constants.⁵¹ However, the softening of E_{2g}^1 vibration and the negligible change of A_{1g} mode indicate the weaker interlayer interactions in MoS₂ cannot be only associated with the van der Waals interactions, instead there are additional interlayer interactions in the material.⁴⁵ The E_{2g}^1 and the A_{1g} vibrations in BNNT@multi-MoS₂NT both softened compared with these two modes in bulk MoS₂, which might reflect the tensile strain in nanotubes does have a strong effect on the phonon dispersion and causes softening of the two active Raman modes.⁵²

Moreover, there are more Raman peaks in Figure 4c using the excitation wavelength of 632.8 nm which is in resonance with the direct band gap (~1.96 eV) of MoS₂ at the K point.⁵³ In the resonant Raman spectra, the most prominent mode around 460 cm⁻¹ arises from a second-order process of involving the longitudinal acoustic phonons at M point (LA(M)).⁵⁰ On the spectrum of BNNT@multi-MoS₂NT, the peaks around 178, 453, and 637 cm⁻¹ were observed as well the E_{2g}^1 (380 cm⁻¹) and A_{1g} (405 cm⁻¹) peaks. The peak at 453 cm⁻¹ is assigned as the double frequency of the LA(M) mode. Moreover the peaks centered at 178 and 637 cm⁻¹ are assigned to $A_{1g} - LA$ and $A_{1g} + LA$ Raman modes, respectively. The shoulder of A_{1g} peak in BNNT@multi-MoS₂NT evolves into an individual peak at 421 cm⁻¹ in BNNT@single-MoS₂NT. This peak has been interpreted through a Raman-inactive mode (B_{1u}) due to a two-photon scattering process involving a longitudinal quasi-acoustic phonon and a transverse optical phonon.⁵⁰ Moreover, on the Raman spectrum of BNNT@single-MoS₂NT, a blue-shift of the E_{2g}^1 (385 cm⁻¹) and A_{1g} (407 cm⁻¹) peaks

was both observed respect to the two modes in BNNT@multi-MoS₂NT. Interestingly, the intensity of $A_{1g} - LA$ and $A_{1g} + LA$ vibration modes become much weaker in BNNT@single-MoS₂NT. Besides, the resonant Raman spectrum of BNNT@single-MoS₂NT is gradually lift-up of background towards high frequencies which is attributed to the tail of the extremely strong PL in single-walled MoS₂ nanotubes. These significant differences of the Raman features between BNNT@single-MoS₂NT and BNNT@multi-MoS₂NT imply that Raman spectroscopy could serve as a reliable tool for identifying single-walled MoS₂ nanotubes.

The absorption spectrum of BNNT@single-MoS₂NT was found to be mostly unaltered, except for a slight blueshift of the resonances (Figure 4b). BNNT@single-MoS₂NT PL peak A at 1.85 eV almost matches the lower absorption resonance in its position (Figure 4d). The PL of BNNT@multi-MoS₂NT was significantly quenched, which indicates multi-walled MoS₂ nanotubes are similar to the bulk MoS₂ having an indirect band gap.

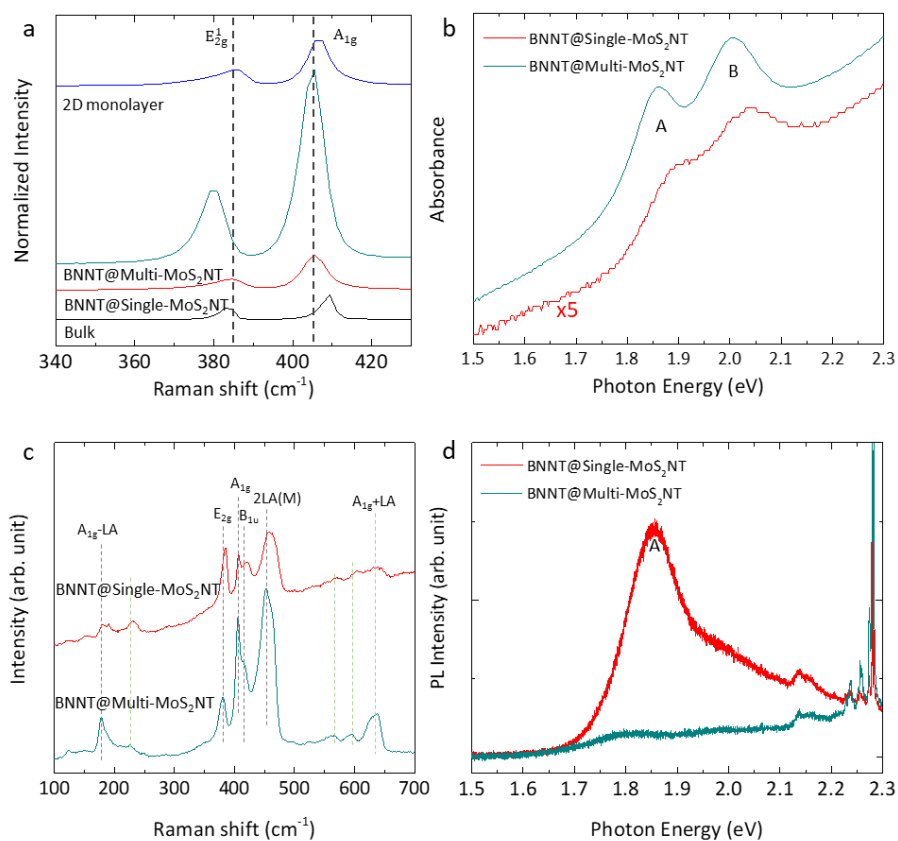


Figure 4. (a) Raman spectra of 2D monolayer MoS₂, BNNT@multi-MoS₂NT, BNNT@single-MoS₂NT, and the bulk MoS₂ with the excitation wavelength of 532 nm. (b) Representative absorption spectra of BNNT@single-MoS₂NT and BNNT@multi-MoS₂NT heteronanotubes. (c) Resonant Raman spectra of BNNT@single-MoS₂NT and BNNT@multi-MoS₂NT heteronanotubes using 632.8 nm laser. (d) PL spectra of BNNT@single-MoS₂NT and BNNT@multi-MoS₂NT heteronanotubes with 532 nm excited laser.

Conclusions

In conclusion, heteronanotubes of single- and multi-walled MoS₂ nanotubes coaxially grown on BNNTs were synthesized in this work. We observed a strong PL from single-walled MoS₂ nanotubes grown on BNNTs, and this result corresponded with our DFT results that large-diameter single-walled MoS₂ nanotubes have direct band gap at K point. Meanwhile, the PL signal of single-walled MoS₂ nanotubes in SWCNT@BNNT@MoS₂NT heteronanotubes is noticeably quenched. The charge and energy transfer between SWCNTs and single-walled MoS₂ nanotubes in one-dimensional van der Waals heterostructures were examined by PL and Raman spectroscopy. The significant PL quenching in multi-walled MoS₂ nanotubes verified their indirect band gap structures. The different Raman features of single- and multi-walled MoS₂ nanotubes under resonant and non-resonant condition may provide a tool for distinguishing the number of walls in MoS₂ nanotubes. The BNNT based hetero structure may pave a way for investigating the optical properties of TMD nanotubes.

Methods

Synthesis of the BNNT Film. The SWCNT film used in this work as a template was synthesized by aerosol CVD and collected on a filter paper.⁵⁴ The SWCNT film with filter paper was dry-transferred onto a ceramic washer (6 mm). After removing the filter paper, the SWCNT film was suspended on the ceramic washer. For the BNNT CVD, the BN precursor, 30 mg of borane-ammonia complex (97%, Sigma-Aldrich), was placed upstream in the quartz tube and heated to 70°C. A low-pressure CVD with 300 Pa was applied here for the reaction at 1075°C and Ar with 3% H₂ was the carrier gas for the BN precursor with a flow rate of 300 sccm. The representative CVD time here was 1 hour and the average coating ratio was around 55%. After the BNNT coating CVD procedure, samples were set in a pure O₂ atmosphere CVD system for thermal oxidizing the inner SWCNT film to obtain the pure BNNT film. The oxidation process was taken at 610°C at 85kPa with a flow rate of 45 sccm O₂ gas for 12 hours.

Growth of the BNNT@MoS₂NT film. The BNNT@MoS₂NT heteronanotube was synthesized by a low-pressure CVD system using sulfur (sublimated, 99.0%, Wako) and MoO₃ (99.9%, Sigma-Aldrich) powders as precursors. Sulfur(S) powder was loaded in a quartz boat and placed out of the furnace at the upstream of the quartz tube chamber. The S quartz boat was heated up by a rubber heater to 138 °C. MoO₃ powder was placed upstream of the substrates and heated up to 530 °C. The BNNT film sample was set downstream of the MoO₃ powder and heated up to 530 °C for synthesizing single-walled MoS₂ nanotubes and 750 °C for multi-walled MoS₂ nanotubes. Ar gas with a flow rate of 50 sccm was introduced into the chamber as a carrier. The typical reaction time at aimed temperature was 10 min. The distance of the MoO₃ quartz boat and the substrate is an essential parameter for controlling the quality of MoS₂. The distance in this experiment was 10 cm.

Optical characterizations and TEM characterizations. The Raman and PL spectra of the samples were obtained by a Raman spectrometer (inVia, Renishaw) with the excitation wavelengths of 532 nm and 632.8 nm. The absorption spectra were measured by a UV-Vis-NIR spectrophotometer (Shimadzu UV-3150). The photo-emission measurements were performed using XPS (PHI5000, Versa Probe) with monochromatic Al K α radiation. The TEM images were obtained by a JEM-2010F microscope and a JEM-2800 microscope at an acceleration voltage of

200 kV or 100 kV. The high-resolution TEM images were taken by a JEM-ARM200F microscope with a thermal field-emission gun operating at 120 kV.

DFT Calculation. The Simulation Tool for Atom Technology (STATE)⁵⁵ package was used for investigating the geometric and electronic structures. General gradient approximation by Perdew-Burke-Ernzerhof functional^{56, 57} was applied to describe exchange correlation potential energy between electrons. Ultrasoft pseudopotentials were used for the pseudopotential between electrons and ions.⁵⁸ Cutoff energies of plane-wave to expand the valence wavefunction and deficit charge density were 340 and 3061 eV (25 and 225 Ry), respectively. Atomic structure was optimized until forces acting on each atom are less than 0.684 eV/nm (1.33×10^{-3} Hartree/au). A lattice parameter along tube direction was fixed to 0.315 nm, which corresponds with the experimental value of bulk MoS₂.⁵⁹ The Brillouin zone integration was carried out under six k points along the tube direction.

Acknowledgements

Part of this work was supported by JSPS KAKENHI Grant Numbers JP18H05329, JP19H02543, JP20H00220, JP20KK0114, JP18J22263 and by JST, CREST Grant Number JPMJCR20B5, Japan. ML acknowledges the support from JSPS Grant-in-Aid for Young Scientist Grant Number JP19J13441. Part of the work was conducted at the Advanced Characterization Nanotechnology Platform of the University of Tokyo, supported by the “Nanotechnology Platform” of the MEXT, Japan, grant numbers JPMXP09A20UT0063.

References

1. Geim, A. K.; Grigorieva, I. V. Van der Waals heterostructures. *Nature* **2013**, 499, 419-425.
2. Wang, Q. H.; Kalantar-Zadeh, K.; Kis, A.; Coleman, J. N.; Strano, M. S. Electronics and optoelectronics of two-dimensional transition metal dichalcogenides. *Nat. Nanotechnol.* **2012**, 7, 699-712.
3. Chhowalla, M.; Shin, H. S.; Eda, G.; Li, L.-J.; Loh, K. P.; Zhang, H. The chemistry of two-dimensional layered transition metal dichalcogenide nanosheets. *Nat. Chem.* **2013**, 5, 263-275.
4. Fiori, G.; Bonaccorso, F.; Iannaccone, G.; Palacios, T.; Neumaier, D.; Seabaugh, A.; Banerjee, S. K.; Colombo, L. Electronics based on two-dimensional materials. *Nat Nanotechnol.* **2014**, 9, 768-779.
5. Jariwala, D.; Sangwan, V. K.; Lauhon, L. J.; Marks, T. J.; Hersam, M. C. Emerging device applications for semiconducting two-dimensional transition metal dichalcogenides. *ACS nano* **2014**, 8, 1102-1120.
6. Zhang, H. Ultrathin two-dimensional nanomaterials. *ACS nano* **2015**, 9, 9451-9469.
7. Liu, Y.; Weiss, N. O.; Duan, X.; Cheng, H.-C.; Huang, Y.; Duan, X. Van der Waals heterostructures and devices. *Nat. Rev. Mater.* **2016**, 1, 1-17.
8. Cui, X.; Lee, G.-H.; Kim, Y. D.; Arefe, G.; Huang, P. Y.; Lee, C.-H.; Chenet, D. A.; Zhang, X.; Wang, L.; Ye, F. Multi-terminal transport measurements of MoS₂ using a van der Waals heterostructure device platform. *Nat. Nanotechnol.* **2015**, 10, 534-540.
9. Tenne, R. Advances in the synthesis of inorganic nanotubes and fullerene-like nanoparticles. *Angew. Chem. Int. Ed.* **2003**, 42, 5124-5132.
10. Xiang, R.; Inoue, T.; Zheng, Y.; Kumamoto, A.; Qian, Y.; Sato, Y.; Liu, M.; Tang, D.; Gokhale, D.; Guo, J. One-dimensional van der Waals heterostructures. *Science* **2020**, 367, 537-542.
11. Feldman, Y.; Wasserman, E.; Srolovitz, D.; Tenne, R. High-rate, gas-phase growth of MoS₂ nested inorganic fullerenes and nanotubes. *Science* **1995**, 267, 222-225.
12. Seifert, G.; Köhler, T.; Tenne, R. Stability of metal chalcogenide nanotubes. *J. Phys. Chem. B* **2002**, 106, 2497-2501.
13. Strojnik, M.; Kovic, A.; Mrzel, A.; Buh, J.; Strle, J.; Mihailovic, D. MoS₂ nanotube field effect transistors. *AIP Adv.* **2014**, 4, 097114.
14. Roxlo, C.; Chianelli, R.; Deckman, H.; Ruppert, A.; Wong, P. Bulk and surface optical absorption in molybdenum disulfide. *J. Vac. Sci. Technol. A* **1987**, 5, 555-557.
15. Tributsch, H. Layer-Type Transition Metal Dichalcogenides — a New Class of Electrodes for Electrochemical Solar Cells. *Berichte der Bunsengesellschaft für physikalische Chemie* **1977**, 81, 361-369.
16. Fortin, E.; Sears, W. Photovoltaic effect and optical absorption in MoS₂. *J. Phys. Chem. Solids* **1982**, 43, 881-884.
17. Li, T.; Galli, G. Electronic properties of MoS₂ nanoparticles. *J. Phys. Chem. C* **2007**, 111, 16192-16196.
18. Mak, K. F.; Lee, C.; Hone, J.; Shan, J.; Heinz, T. F. Atomically thin MoS₂: a new direct-gap semiconductor. *Phys. Rev. Lett.* **2010**, 105, 136805.
19. Splendiani, A.; Sun, L.; Zhang, Y.; Li, T.; Kim, J.; Chim, C.-Y.; Galli, G.; Wang, F. Emerging photoluminescence in monolayer MoS₂. *Nano Lett.* **2010**, 10, 1271-1275.
20. Eda, G.; Yamaguchi, H.; Voiry, D.; Fujita, T.; Chen, M.; Chhowalla, M. Photoluminescence from chemically exfoliated MoS₂. *Nano Lett.* **2011**, 11, 5111-5116.
21. Seifert, G.; Terrones, H.; Terrones, M.; Jungnickel, G.; Frauenheim, T. Structure and electronic properties of MoS₂ nanotubes. *Phys. Rev. Lett.* **2000**, 85, 146.
22. Zhang, D.-B.; Dumitrică, T.; Seifert, G. Helical nanotube structures of MoS₂ with intrinsic twisting: an objective molecular dynamics study. *Phys. Rev. Lett.* **2010**, 104, 065502.
23. Zibouche, N.; Kuc, A.; Heine, T. From layers to nanotubes: Transition metal disulfides TMS₂. *The Eur. Phys. J. B* **2012**, 85, 49.

24. Milošević, I.; Nikolić, B.; Dobardžić, E.; Damnjanović, M.; Popov, I.; Seifert, G. Electronic properties and optical spectra of MoS₂ and WS₂ nanotubes. *Phys. Rev. B* **2007**, *76*, 233414.
25. Zhu, Y. Q.; Hsu, W. K.; Kroto, H. W.; Walton, D. R. M. Carbon nanotube template promoted growth of NbS nanotubes/nanorods. *Chem. Commun.* **2001**, 2184-2185.
26. Whitby, R. L.; Hsu, W. K.; Fearon, P. K.; Billingham, N. C.; Maurin, I.; Kroto, H. W.; Walton, D. R.; Boothroyd, C. B.; Firth, S.; Clark, R. J. Multiwalled carbon nanotubes coated with tungsten disulfide. *Chem. Mater.* **2002**, *14*, 2209-2217.
27. Meyer, R. R.; Sloan, J.; Dunin-Borkowski, R. E.; Kirkland, A. I.; Novotny, M. C.; Bailey, S. R.; Hutchison, J. L.; Green, M. L. Discrete atom imaging of one-dimensional crystals formed within single-walled carbon nanotubes. *Science* **2000**, *289*, 1324-1326.
28. Philp, E.; Sloan, J.; Kirkland, A. I.; Meyer, R. R.; Friedrichs, S.; Hutchison, J. L.; Green, M. L. An encapsulated helical one-dimensional cobalt iodide nanostructure. *Nat. Mater.* **2003**, *2*, 788-791.
29. Koroteev, V.; Bulusheva, L.; Asanov, I.; Shlyakhova, E.; Vyalikh, D.; Okotrub, A. Charge transfer in the MoS₂/carbon nanotube composite. *J. Phys. Chem. C* **2011**, *115*, 21199-21204.
30. Burdanova, M. G.; Kashtiban, R. J.; Zheng, Y.; Xiang, R.; Chiashi, S.; Woolley, J. M.; Staniforth, M.; Sakamoto-Rablah, E.; Xie, X.; Broome, M. Ultrafast Optoelectronic Processes in 1D Radial van der Waals Heterostructures: Carbon, Boron Nitride, and MoS₂ Nanotubes with Coexisting Excitons and Highly Mobile Charges. *Nano Lett.* **2020**, *20*, 3560-3567.
31. Wang, Y.; Ma, Z.; Chen, Y.; Zou, M.; Yousaf, M.; Yang, Y.; Yang, L.; Cao, A.; Han, R. P. Controlled Synthesis of Core-Shell Carbon@ MoS₂ Nanotube Sponges as High - Performance Battery Electrodes. *Adv. Mater.* **2016**, *28*, 10175-10181.
32. Dresselhaus, M. S.; Dresselhaus, G.; Saito, R.; Jorio, A. Raman spectroscopy of carbon nanotubes. *Phys. Rep.* **2005**, *409*, 47-99.
33. Lefebvre, J.; Fraser, J.; Finnie, P.; Homma, Y. Photoluminescence from an individual single-walled carbon nanotube. *Phys. Rev. B* **2004**, *69*, 075403.
34. Golberg, D.; Bando, Y.; Tang, C.; Zhi, C. Boron nitride nanotubes. *Adv. Mater.* **2007**, *19*, 2413-2432.
35. Lee, C. H.; Xie, M.; Kayastha, V.; Wang, J.; Yap, Y. K. Patterned growth of boron nitride nanotubes by catalytic chemical vapor deposition. *Chem. Mater.* **2010**, *22*, 1782-1787.
36. Virsek, M.; Krause, M.; Kolitsch, A.; Remškar, M. Raman characterization of MoS₂ microtube. *Phys. Status Solidi (b)* **2009**, *246*, 2782-2785.
37. Coehoorn, R.; Haas, C.; De Groot, R. Electronic structure of MoSe₂, MoS₂, and WSe₂. II. The nature of the optical band gaps. *Phys. Rev. B* **1987**, *35*, 6203.
38. Kam, K.; Parkinson, B. Detailed photocurrent spectroscopy of the semiconducting group VIB transition metal dichalcogenides. *J. Phys. Chem.* **1982**, *86*, 463-467.
39. Evans, B.; Young, P. Optical absorption and dispersion in molybdenum disulphide. *P. Roy. Soc. A-Math. Phys.* **1965**, *284*, 402-422.
40. Froehlicher, G.; Lorchat, E.; Berciaud, S. Charge versus energy transfer in atomically thin graphene-transition metal dichalcogenide van der Waals heterostructures. *Phys. Rev. X* **2018**, *8*, 011007.
41. Mak, K. F.; He, K.; Lee, C.; Lee, G. H.; Hone, J.; Heinz, T. F.; Shan, J. Tightly bound trions in monolayer MoS₂. *Nat. Mater.* **2013**, *12*, 207-211.
42. Mouri, S.; Miyauchi, Y.; Matsuda, K. Tunable photoluminescence of monolayer MoS₂ via chemical doping. *Nano Lett.* **2013**, *13*, 5944-5948.
43. Rao, A. M.; Eklund, P.; Bandow, S.; Thess, A.; Smalley, R. E. Evidence for charge transfer in doped carbon nanotube bundles from Raman scattering. *Nature* **1997**, *388*, 257-259.
44. Corio, P.; Santos, P.; Brar, V.; Samsonidze, G. G.; Chou, S.; Dresselhaus, M. Potential dependent surface Raman spectroscopy of single wall carbon nanotube films on platinum electrodes. *Chem. Phys. Lett.* **2003**, *370*, 675-682.

45. Lee, C.; Yan, H.; Brus, L. E.; Heinz, T. F.; Hone, J.; Ryu, S. Anomalous lattice vibrations of single- and few-layer MoS₂. *ACS nano* **2010**, 4, 2695-2700.
46. Kohn, W.; Sham, L. J. Self-consistent equations including exchange and correlation effects. *Phys. Rev.* **1965**, 140, A1133.
47. Hohenberg, P.; Kohn, W. Inhomogeneous electron gas. *Phys. Rev.* **1964**, 136, B864.
48. Hisama, K.; Maruyama, M.; Chiashi, S.; Maruyama, S.; Okada, S. Indirect-to-direct band gap crossover of single walled MoS₂ nanotubes. *arXiv preprint arXiv:2011.09103* **2020**.
49. Bertrand, P. Surface-phonon dispersion of MoS₂. *Phys. Rev. B* **1991**, 44, 5745.
50. Li, H.; Zhang, Q.; Yap, C. C. R.; Tay, B. K.; Edwin, T. H. T.; Olivier, A.; Baillargeat, D. From bulk to monolayer MoS₂: evolution of Raman scattering. *Adv. Funct. Mater.* **2012**, 22, 1385-1390.
51. Bagnall, A.; Liang, W.; Marseglia, E.; Welber, B. Raman studies of MoS₂ at high pressure. *Phys. B+C* **1980**, 99, 343-346.
52. Ghorbani-Asl, M.; Zibouche, N.; Wahiduzzaman, M.; Oliveira, A. F.; Kuc, A.; Heine, T. Electromechanics in MoS₂ and WS₂: nanotubes vs. monolayers. *Sci. Rep.* **2013**, 3, 2961.
53. Windom, B. C.; Sawyer, W.; Hahn, D. W. A Raman spectroscopic study of MoS₂ and MoO₃: applications to tribological systems. *Tribol. Lett.* **2011**, 42, 301-310.
54. Nasibulin, A. G.; Kaskela, A.; Mustonen, K.; Anisimov, A. S.; Ruiz, V.; Kivisto, S.; Rackauskas, S.; Timmermans, M. Y.; Pudas, M.; Aitchison, B. Multifunctional free-standing single-walled carbon nanotube films. *ACS nano* **2011**, 5, 3214-3221.
55. Morikawa, Y.; Iwata, K.; Terakura, K. Theoretical study of hydrogenation process of formate on clean and Zn deposited Cu (1 1 1) surfaces. *Appl. Surf. Sci.* **2001**, 169, 11-15.
56. Perdew, J. P.; Burke, K.; Ernzerhof, M. Generalized gradient approximation made simple. *Phys. Rev. Lett.* **1996**, 77, 3865.
57. Perdew, J. P.; Burke, K.; Ernzerhof, M. Generalized Gradient Approximation Made Simple [Phys. Rev. Lett. 77, 3865 (1996)]. *Phys. Rev. Lett.* **1997**, 78, 1396-1396.
58. Vanderbilt, D. Soft self-consistent pseudopotentials in a generalized eigenvalue formalism. *Phys. Rev. B* **1990**, 41, 7892.
59. Wakabayashi, N.; Smith, H.; Nicklow, R. Lattice dynamics of hexagonal MoS₂ studied by neutron scattering. *Phys. Rev. B* **1975**, 12, 659.